

Full Length Article

NiB monolayer: A topological metal with high NORR electrocatalytic performance

Wengeng Chen^a, Yaowei Xiang^a, Zepeng Wu^a, Meijie Wang^a, Yimei Fang^a, Zi-Zhong Zhu^a, Shunqing Wu^a, Xinrui Cao^{a,b,*}

^a Department of Physics, Xiamen University, Xiamen 361005, China

^b Fujian Provincial Key Laboratory of Theoretical and Computational Chemistry, Xiamen University, Xiamen 361005, China



ARTICLE INFO

Keywords:

NO electrochemical reduction
Ammonia synthesis
NiB monolayer
First-principles calculations
Topological metal
Constant-potential method

ABSTRACT

Electrochemical reduction reaction of NO (NORR) offers a promising strategy for effective removal of NO coupled with synthesis of NH₃. In this study, the newly reported NiB monolayer with topological metal properties is proved to have excellent catalytic activity and high selectivity toward NO-to-NH₃ conversion by using density functional theory (DFT) and the constant potential method (CPM). Calculations reveal that the peculiar building blocks of Ni-B triangles and tetragons can facilitate NO adsorption and activation via an electron donation-back-donation interaction mechanism. The predicted free energy profiles of the four considered NORR pathways toward synthesis of NH₃ are generally going downhill under the applied potential of 0 V, and an optimal reduction pathway was screened out with a maximum kinetic barrier of 0.16 eV during the hydrogenation process. The low adsorption free energy of H atom together with the existing relatively higher energy barriers for the formation of N₂O/N₂ guarantee the hydrogen evolution reaction (HER) and the partial reduction channel are less competitive than NH₃ production. These findings enrich the potential application of two dimensional topological materials in electrocatalysis.

1. Introduction

As a major air pollutant, nitric oxide has caused serious environmental problems [1,2], and it is also a great threat to human health [3]. Therefore, nitric oxide capture and removal has received considerable attention. Currently, selective catalytic reduction (SCR) is acknowledged as the most effective way to remove NO [4,5]. However, this approach is uneconomical and environmentally unfriendly due to the high energy demand and significant consumption of costly reducing agents [6,7]. Additionally, ammonia is an important raw material for industrial and agricultural fields [8,9], and its industrial production still heavily relies on the traditional Haber-Bosch process, which is an energy-intensive production process with a large amount of CO₂ release [10,11]. To address these issues, an alternative approach for NH₃ synthesis, that is, the electrochemical reduction of nitrogen to produce ammonia has been proposed [12–19]. Due to the inert chemical properties and low solubility of nitrogen, the electrochemical N₂ reduction reaction (NRR) still faces a significant challenge in the practical application [20–22].

Very recently, a new scheme to generate ammonia through the electrochemical reduction reaction of nitric oxide (NORR) has been proposed. This method not only removes the harmful NO, but also produces the value-added ammonia [23–25]. By now, some catalysts such as pure metal-based catalysts (Pt [26,27], Au [28], Cu [23]), single atom catalysts (TM-Pt (1 0 0) (TM = Ti, Cr, Co, Ni) [29], Zr-C₂N [30], Co-Pc sheet [31], Si-N₄ embedded graphene [32], Cu@g-C₃N₄ [33], B@graphene [34]) and biatom catalysts (Cr₂-C₂N [35]) have been exploited for NORR.

Two-dimensional transition metal boride (MBene) has gained attention in recent years due to their intriguing properties [36], including their large exposed surface area and good electrical conductivity, making them potential candidates for battery electrode materials, electrocatalysts [37–42], spintronics [43], and other fields. Topological materials [44,45], especially those in their two dimensional (2D) form showing high catalytic activity in some electrochemical reactions due to their robust topological surface states or edge states [46–49]. Recently, we reported a two-dimensional NiB monolayer topological material with thermodynamic and mechanical stability using the AGA method [50],

* Corresponding author at: Department of Physics, Xiamen University, Xiamen 361005, China.

E-mail address: xinruicao@xmu.edu.cn (X. Cao).

<https://doi.org/10.1016/j.apsusc.2023.157887>

Received 8 May 2023; Received in revised form 24 June 2023; Accepted 25 June 2023

Available online 26 June 2023

0169-4332/© 2023 Elsevier B.V. All rights reserved.

and the electronic properties of NiB monolayer can be manipulated through strain modulation. Previous experimental research had proved that it is possible to obtain 2D NiB with various thickness from the Li deintercalation of layered LiNiB [51]. To date, the use of this novel 2D MBene NiB monolayer with topological properties in electrocatalysis has not been studied yet.

In this paper, we explore the catalytic mechanism of 2D NiB material in the NORR by using density functional theory (DFT) and the constant potential method (CPM). We systematically investigate the NO adsorption and activation on NiB monolayer, and the possible reduction paths for NORR. After considering the corresponding limiting potentials and the kinetic barriers, the most favorable reduction route was screened out. Our results show that the NiB monolayer can effectively capture and activate the NO molecule, and the existence of relative high energy barriers for two *N and two *NO coupling limits the N₂ and N₂O generation. Additionally, the low adsorption free energy of H atom on NiB monolayer suppresses the competition reaction of the hydrogen evolution reaction (HER). We hope our results provide new insights for the removal of NO and the ammonia generation.

2. Computational details

In this work, all calculations were carried out using the Vienna Ab initio Simulation Package (VASP) based on spin-polarized density functional theory [52,53]. The projector augmented-wave (PAW) method was used to describe the ion-electron interaction [54]. The Perdew-Burke-Ernzerhof (PBE) generalized gradient approximation (GGA) was used to describe exchange correlation [55]. The DFT-D3 method was used to evaluate van der Waals interactions between the substrates and adsorbates [56,57]. A 3 × 2 supercell was used to model the NiB monolayer, including 24 Ni atoms and 24 B atoms. To minimize the mutual influence between adjacent periodic layers, a 20 Å vacuum space was chosen in the z direction. The cutoff energy of the electronic plane-wave was set to 500 eV. The energy and the force convergence criteria were set to 1 × 10⁻⁵ eV and 0.02 eV/Å, respectively. The Monkhorst-Pack k-point grid of 3 × 2 × 1 and 8 × 7 × 1 were used for geometric optimization and electronic properties calculation, respectively. Ab initio molecular dynamics (AIMD) simulations [58] were performed at 300 K using the canonical ensemble (NVT) method, with a time step of 2 fs and a total period of 20 ps. The climbing-image nudged elastic band (CI-NEB) method [59] was employed to search the transition states during the NORR, and the force convergence criterion was set as 0.03 eV/Å. The adsorption energy (E_{ad}) was defined as follows:

$$E_{ad} = E_{\text{support+adsorbate}} - E_{\text{support}} - E_{\text{adsorbate}} \quad (1)$$

where $E_{\text{support+adsorbate}}$ was the total energies of adsorbed systems, and the E_{support} and $E_{\text{adsorbate}}$ represented the energies of the individual support and the isolated adsorbates, respectively. The computational hydrogen electrode (CHE) model [60] was used to calculate the Gibbs free energy change (ΔG) of each basic step of NO electrochemical reduction. The ΔG was described as the following:

$$\Delta G = \Delta E + \Delta E_{ZPE} - T\Delta S + \Delta G_U + \Delta G_{pH} \quad (2)$$

where ΔE is the change of the total electronic energy which can be calculated by DFT calculations, ΔE_{ZPE} and $T\Delta S$ are zero-point energy and the entropy of each basic reaction at the temperature T (T = 298.15 K). ΔG_U is the influence of the applied electrode potential U on the free energy, and ΔG_{pH} symbolized the free energy correction of pH, which was calculated by using the equation $\Delta G_{pH} = k_B T \times \ln 10 \times \text{pH}$. Here, k_B is the Boltzmann constant, and pH is 0 in an acidic medium. The entropies of gas molecules (NO, NH₃, and H₂) are sourced from the NIST database [61]. We assessed the solvation effect using VASPsol code with a dielectric constant of 80 [62] to simulate the water environment. Furthermore, we utilized the JDFTx code [63] to evaluate the effect of both aqueous environment and the applied electrode potential on

NORR. The grand free energy was determined using the JDFTx code with the constant potential method (CPM) [64], the energy cutoff and the convergence criteria of electronic energies was set to 20 and 10⁻⁸ Hartree, respectively. The core-valence interactions were treated by the PBE-D3 functional [57]. The charge-asymmetry corrected, local-response, and nonlocal-cavity (CANDLE) solvation model [65] was used to account for solvation effects. During the calculation, the total net charges of the system vary at the atomic level to match the electrode potential. The change in free energy of each fundamental step was calculated using the following equation [64]:

$$\Delta G_{CPM} = G(I_2) - G(I_1) - G(H_2(g))/2 + |e|U - (q_1 - q_2)\mu_e \quad (3)$$

where the $G(I_1)$ and $G(I_2)$ represented the free energies of the reactants and products at the applied potentials (U) versus the standard hydrogen electrode (SHE), and the $G(H_2(g))$ was the free energy of the hydrogen. The total net charges of the reactants and products were represented by q_1 and q_2 , respectively, and the electron energy at the electrode potential was symbolized by μ_e .

3. Results and discussion

3.1. Adsorption of gas molecules on NiB

The optimized NiB monolayer structure and its representative adsorption sites are presented in Fig. 1a and 1b. According to the symmetry of NiB and three typical adsorption sites, that are, top site, bridge site, and hollow site, we finally considered eight adsorption sites, as depicted in Fig. 1b. Ten common gas molecules including H₂, H₂O, O₂, CO, NO, NO₂, NH₃, CO₂, H₂S and N₂ are considered here to study the adsorption behavior of NiB. Several typical adsorption orientations with different adsorption terminal are all considered. The adsorption energy for the optimal adsorption configurations of these aforementioned ten molecules were illustrated in Fig. 1c. Clearly, the NiB monolayer possesses relative strong adsorption capabilities towards CO, NO, NO₂, NH₃ and H₂S. Among these gases, the adsorption energy for NO is the largest (-1.62 eV), highlighting NiB's superior capacity for nitric oxide capture. In order to consider the influence of adsorbates on each other in our study, we performed calculations using larger cell sizes, including 5 × 4 and 4 × 3 supercells, to evaluate and compare the adsorption behavior. Interestingly, our calculations (Fig. S1) show that the NO adsorption energy (-1.62 eV and -1.60 eV) on these larger cells is equivalent to that on 3 × 2 supercells (-1.62 eV). Based on this analysis, we conclude that the 3 × 2 supercell effectively reflects the catalytic process.

It is known that the effective adsorption of NO is the first crucial step during the NORR process. Among the considered adsorption patterns, the NO molecule takes an inclined adsorption configuration with N-end adsorbed on the H2 site is the most stable adsorption mode. To better understanding the NO-NiB interaction, we plot the partial density of states (PDOS) of NO, the bonded Ni and B atoms before and after NO adsorption and the charge density difference of NO adsorbed NiB in Fig. 2a and 2b, respectively. It can be seen that the NO-2p orbital significantly hybridizes with B-2p and Ni-3d orbitals, indicating a strong interaction between NO and NiB monolayer, and the Bader charge analysis reveals that the adsorbed NO accepts 1.02 e from NiB substrate. The formation of chemical bonding between NO and NiB monolayer originates from an electron donation/back-donation mechanism. As presented from the obtained charge density differences for the adsorbed system, the electron accumulation and depletion both occurs on the adsorbed NO and the NiB monolayer. To be more specific, Ni-3d and B-2p orbitals donate electrons to the partial occupied NO-π* orbital while the NO-σ orbital donates electrons to Ni-3d and B-2p orbitals. The bidirectional charge transfer mode weakens the N-O bond, leading to the increase of the N-O bond length from 1.17 Å (free NO molecule) to around 1.22 Å, suggesting that the NO is activated by NiB monolayer. Noted that, the adsorption energies of NO on Ni(111) surface [66] and

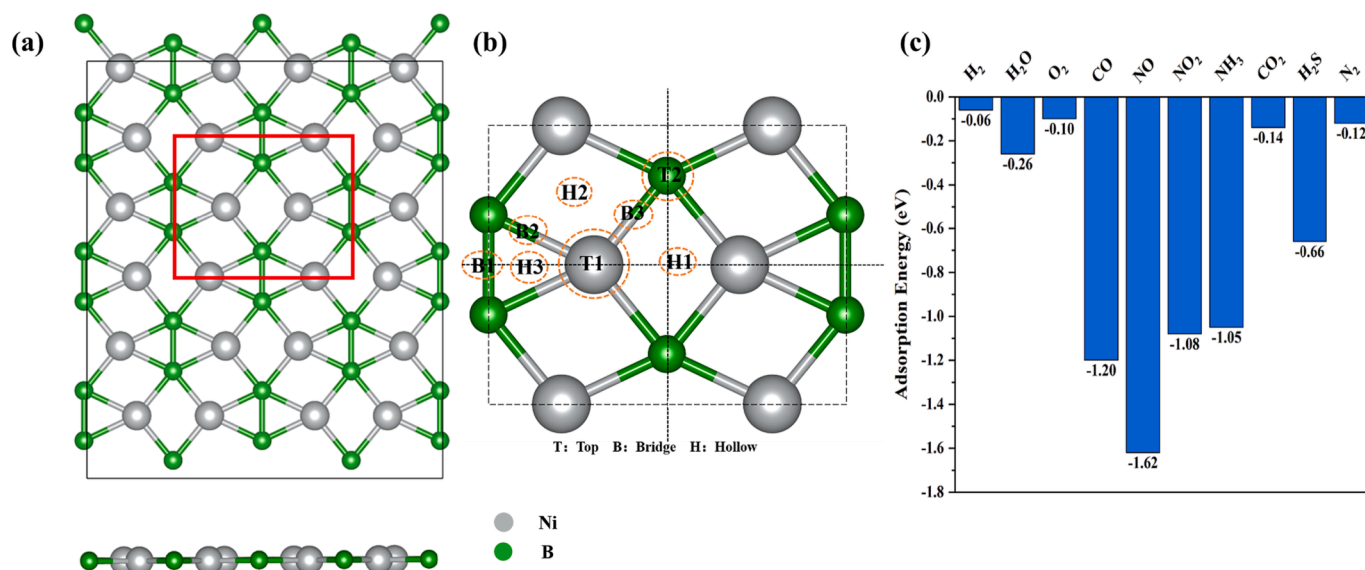


Fig. 1. (a) Top-view and side-view of the optimized NiB monolayer. (b) Representative adsorption sites on NiB monolayer. (c) Adsorption energy of common gas molecules on NiB monolayer. Here, Ni and B atoms are represented by silver and green spheres. (For interpretation of the references to colour in this figure legend, the reader is referred to the web version of this article.)

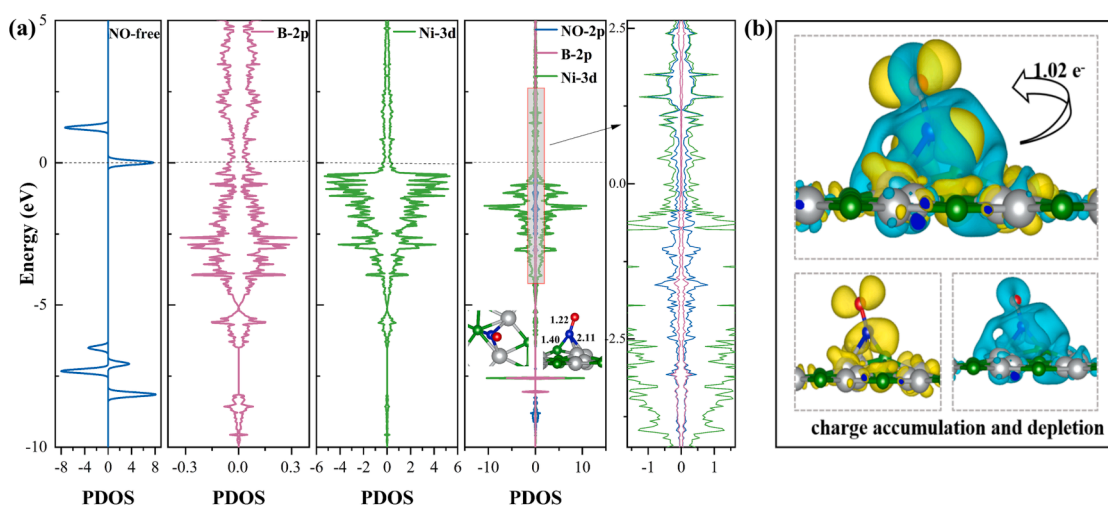


Fig. 2. (a) Partial density of states (PDOS) of NO-2p, B-2p and Ni-3d orbitals before and after NO adsorption on NiB monolayer. Here, only the directly bonded B and Ni atoms are involved. (b) The charge density difference of NO adsorbed NiB. The isosurface value is set to 0.001 e Å⁻³, and the accumulation and depletion charges are shown in yellow and cyan, respectively. The silver, green, blue and red spheres represent Ni, B, N and O atoms, respectively. (For interpretation of the references to colour in this figure legend, the reader is referred to the web version of this article.)

Borophene [67] are -2.48 eV and -1.08 eV, respectively. Too strong or too weak adsorption are both negative effects for catalysis. While for NiB monolayer, the building blocks of Ni-B triangles and tetragons may lead to some peculiar bonding characteristics and give rise to a moderate adsorption of NO on NiB monolayer, which is beneficial for NO activation and the desorption of the corresponding reduction product.

3.2. Electrochemical reduction of NO to NH₃

Starting from the most stable adsorption configuration of NO (see Fig. 2b) on NiB monolayer, we then investigated the conversion of NO to NH₃ through four primary reaction pathways: N-distal, O-distal, N-alternating, and O-alternating (as shown in Fig. 3a). To identify the optimal pathway, we initially optimized the possible configurations of all intermediates during the NORR (Fig. S2a) using VASP.

It is known that the electrocatalysts are usually charged by

accepting/donating electrons from/to the electrodes to match their Fermi level with the applied external potential in reality [64], and the existence of charge effects in 2D system are relatively strong [68–70], which may affect the electrochemical catalytic reactions to some extent. Herein, the CPM method [64,71] implemented in JDFTx software was utilized to compute the free energy variations of intermediates of all fundamental steps (Table S1) obtained from the VASP results to include the impact of the charge effects on the NORR. The calculated NORR free energy diagram of all considered pathways are displayed in Fig. 3c and Fig. S3. Based on Fig. 3c and S3, all the reaction steps involved in the hydrogenation of NiB to produce NH₃ are downhill at the applied potential of 0 V. Generally, the limiting potential (U_L) is a critical parameter in electrocatalysis to evaluate electrocatalysts' activity, and it can be calculated from the maximum Gibbs free energy during the whole reaction steps [72,73]. The NORR exhibits comparatively easier dynamics and thermodynamics compared to the NRR, as NRR typically

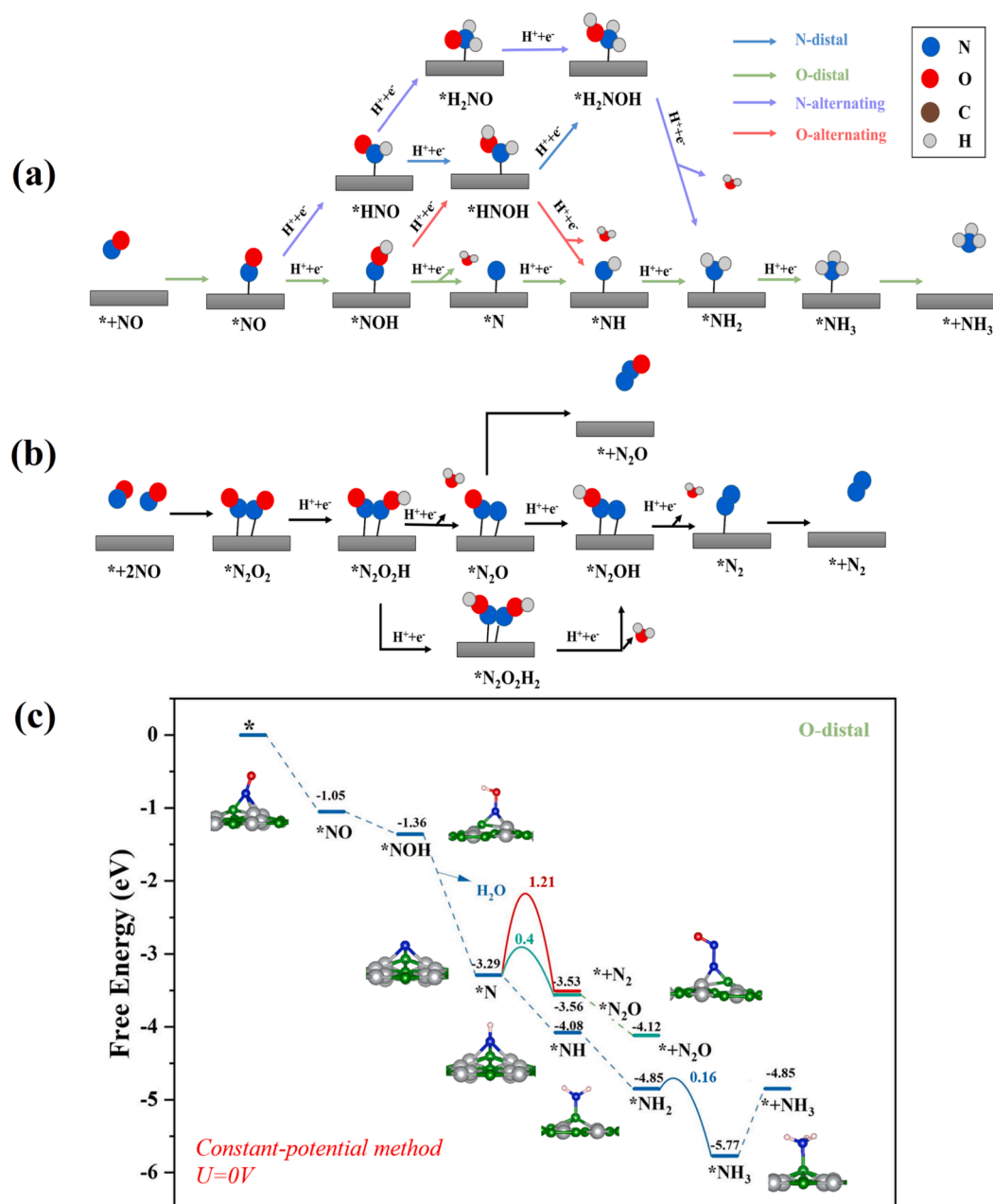


Fig. 3. Schematic illustration of the possible reaction pathways of the NORR toward NH₃ (a) and N₂/N₂O (b). (c) Optimized intermediates and the relative Gibbs free energies for the possible intermediates generated during NO reduction on NiB under the applied potential of 0 V.

requires relatively higher potential and exhibits lower activity due to the chemical inertness of N₂ [12,22] and the activity of NO. For most of the reported NORR electrocatalysts, their limiting potentials ranges from -0.05 to -0.37 V [30,32-35,42,48,74-79] (Table S2). Clearly, the electrocatalytic activity of 2D NiB monolayer is comparable or superior to these NORR electrocatalysts.

Considering that the adsorption free energy of NH₃ is relatively lower than that of NO, and the presence of NO can further promote the NH₃ desorption, which prevents the poisoning of NiB monolayer by the generated *NH₃. As the reduction proceeds, more NH₃ generated on NiB monolayer, giving rise to a decreased average adsorption energy of NH₃ (-0.66, -0.60, -0.52 and -0.47 eV for 5, 6, 7 and 8 NH₃ adsorption, respectively), which is lower than the adsorption energy of a single NH₃ molecule on Ni atoms (-0.76 eV) or B atoms (-1.05 eV). Using an explicit solvation model with 10 H₂O, we performed AIMD simulations to study 8 NH₃ desorption behavior on NiB monolayer at 300 K. The

total simulation time was 20 ps with a time step of 2 fs. As depicted in Fig. S4a, the N1 to N8 molecules and the directly bonded Ni and B atoms are labelled, respectively. The evolution of the B-N and Ni-N bond lengths are shown in Fig. S4b-i. It can be seen that the Ni-N distances in Fig. S4g-i are larger than 4 Å, indicating that three NH₃ molecules desorbed from the surface. Snapshots from the 20 ps AIMD simulation in different views are presented in Fig. S5. To ensure statistical validity, an independent AIMD simulation was carried out with the same initial conditions and settings, and similar results were observed in Fig. S6. Additionally, previous investigations revealed that the generated NH₃ could be further hydrogenated to NH₄⁺ with minor impediment under an acidic environment [26,80]. Based on these, the generated *NH₃ may not be a problem and the NiB monolayer exhibits high catalytic activity for NORR.

We also employed the VASPsol code to compute the free energy changes of the abovementioned reaction pathways for comparison. The

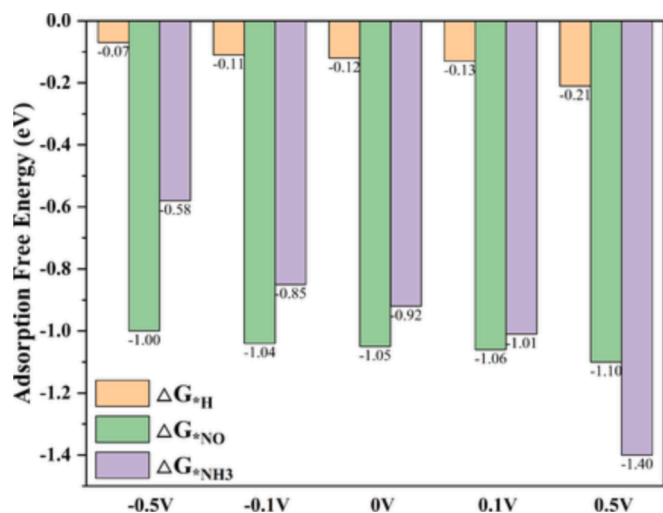


Fig. 4. The calculated adsorption free energies of H atoms, NO molecules, and NH_3 molecules on NiB monolayer.

obtained free energy values are listed in Table S3 and the corresponding free energy diagram is displayed in Fig. S2b. From Fig. S2b, one can see that the trend of the calculated Gibbs free energy profile is consistent with the JDFTx results except for the initial hydrogenation step. According to the JDFTx results, the NiB monolayer is charged by accepting around 3.90 electrons from the electrodes under the applied potential of 0 V and the total net charges of the $*NO$, $*NOH$ and $*HNO$ are decreased to -3.75 e, -3.49 e and -3.78 e, respectively. Then, we evaluated the energy of $*NOH$ and $*HNO$ under different charge states using VASPsol code. When the adsorbed surface is negatively charged with 3 electrons, the energy of $*HNO$ is 0.01 eV lower than that of $*NOH$, and the energy difference is increased to 0.18 eV when four electrons are added in the adsorbed system. Thus, the negatively charged system is beneficial for the stability of the hydrogenated products, especially for $*HNO$, and the difference in the first hydrogenation of NO can be ascribed to the existence of the charge effects under actual voltage conditions that the traditional charge-neutral method based on VASPsol code did not taken into account.

As reported by the experimental research, the stacking of NiB monolayer can lead to the formation of double $[NiB]_2$ and triple $[NiB]_3$ layers through the covalent bonding during the deintercalation of Li from layered $LiNiB$, and the double layer stacking mode is the main product for the condensation of single $[NiB]$ layers [51]. Hence, we fully optimized the double $[NiB]_2$ layers (see Fig. S7a) and evaluated the free energy variations for the NO-to- NH_3 conversion on $[NiB]_2$ following the O-distal reduction pathway. The corresponding intermediates and the Gibbs free energy profile diagram are depicted in Fig. S7b-c. Similar to the NiB monolayer, all fundamental hydrogenation steps are exothermic, ensuring the catalytic effectiveness of NORR on $[NiB]_2$.

As is commonly acknowledged, the kinetic barrier plays a vital role in catalytic reactions, which provides valuable insights into the understanding of the reaction mechanism and highlights the rate-determining step (RDS). Thus, it is necessary to explore the energy barriers for the hydrogenation steps involved in the considered pathways for the NORR as presented in Table S1. For simplicity's sake, the simplest form of a hydrated proton in an aqueous environment, that is H_3O^+ , was employed in our simulations, with the entire system charged with a positive charge by removing one electron from the total electrons. After locating the transition state (TS) structures for these hydrogenation processes using the CI-NEB method, we then calculated the corresponding energies using JDFTx, and the related results are presented in the Fig. S8.

The initial hydrogenation of $*NO$ can result in two intermediates, that are, $*NOH$ and $*HNO$, depending on whether hydrogenation occurs

on the nitrogen or oxygen atom. The generation of $*NOH$ proceeds smoothly with a free energy change of -0.31 eV and this process is barrierless. While for the $*HNO$ formation, it has an energy barrier of 0.65 eV, and the relatively high energy barrier hinders such hydrogenation process. In addition, we also evaluated the hydrogenation barriers for $*HNO$ and $*NOH$ using a neutral H atom adsorbed on the top of the nearest B atom, and the obtained results are presented in Fig. S9. From it, one can see that there is a substantial kinetic barrier for the $*HNO$ (1.51 eV) generation while the energy barrier for $*NO$ to $*NOH$ is 0.85 eV. Therefore, the first hydrogenation reaction (H^+/e^-) towards $*NOH$ is more preferred. When the $*NOH$ formed, the further hydrogenation can undergo two pathways, one of which leads to $*HNOH$ while the other one results in $*N$ upon the removal of H_2O . The former one is exothermic by 0.83 eV, but with an energy barrier of 0.31 eV. In contrast, the latter one is also barrier free and it releases a large energy of -1.93 eV. Hence, $*NOH$ is more inclined to be hydrogenated and then dehydrated to generate $*N$. Subsequently, the formation of $*NH$ and $*NH_2$ are also barrierless. The hydrogenation of $*NH_2$ to $*NH_3$ is the RDS for the O-distal pathway starting from $*NOH$ which only possesses a small energy barrier of 0.16 eV, and with an energy release of 0.92 eV. Calculated MEP for these reaction processes without energy barrier in the O-distal pathway can be seen in Fig. S10. The predicted free energy profiles of the other three pathways are given in Fig. S3.

Considering the potential influence of high NO coverage on the performance of NO-to- NH_3 conversion, our study primarily focuses on two key aspects: the initial hydrogenation reaction of NO at high concentrations and the hydrogenation step with the maximum activation energy along the optimal pathway, specifically, the conversion of $*NH_2$ to $*NH_3$. Based on these results (Fig. S11-S12), we can conclude that the relatively high concentration of NO has little effect on the performance of NO-to- NH_3 conversion.

3.3. NH_3 selectivity

During the NORR process, the main byproducts are N_2O and N_2 . Minimizing the byproduct production is critical for ensuring high selectivity towards the desired product. Noted that, the generated $*N$ can still undergo further reduction to generate N_2O (N-NO coupling) and N_2 (N-N coupling), which are two competing processes, and the activation energy barriers with the corresponding transition states are given in Fig. S8f-g. Compared with the barrier free process for the hydrogenation of $*N$ to $*NH$, N-N and N-NO couplings require an energy barrier of 1.21 eV and 0.40 eV, respectively. The existing kinetic barriers can effectively inhibit these two competing processes.

It is known that N_2O and N_2 can also be obtained through further hydrogenation after NO coupling under high NO coverage, and the key precursor in the formation of N_2O and N_2 is the NO dimer (N_2O_2) formation, and the $O=NN=O$ with a cis form was reported as the most stable configuration [81]. Our study only focuses on the transformation of NO into N_2O and N_2 on NiB monolayer starting with the 2 N-side configurations of N_2O_2 since the 2O-side adsorption on NiB monolayer is not stable in our cases, which is also consistent with our calculation that NO cannot be chemisorbed on NiB monolayer through the O-end adsorption mode. The kinetic barrier for two $*NO$ coupling is 0.47 eV as shown in Fig. S13a. Starting from the $*N_2O_2$, we then explore the subsequent reduction process towards N_2O and N_2 . The optimized structures and the corresponding free-energy diagrams are shown in Fig. S13. The plausible reduction pathway to produce N_2 can be described as $*N_2O_2 \rightarrow *N_2O_2H \rightarrow *N_2O \rightarrow *N_2OH \rightarrow *N_2$ and such processes are downhill in energy.

We also perform AIMD calculations to evaluate the adsorption of NO molecules on NiB substrate under a high concentration of NO at 300 K. When putting 12 NO molecules in the simulated supercell, all NO molecules are isolated chemisorbed on NiB monolayer due to the existence of numerous active sites, as shown in Fig. S14. When the number of NO molecules increase to 24 (see Fig. S15), two NO dimers are observed, one

is chemisorbed and the other one is suspended without directly contact with the NiB monolayer, and the probability of the NO dimer occurrence is relatively low. Combined with the fact that there is a certain energy barrier for the coupling two *NO to yield N_2O_2 , it can be concluded that, the formation of N_2O and N_2 can be prevented by the kinetic barrier and the NO flux controlling.

Another competitive reaction during the NORR is the hydrogen evolution reaction (HER). In our system, we evaluated the possible adsorption of H on NiB monolayer and finally we obtained two representative adsorption configurations, and the corresponding Gibbs free energy (ΔG_{*H}) are shown in Fig. S16. It is evidently that the H atom adsorption is rather weak on NiB monolayer. Thus, the competitive HER can be effectively inhibited. Furthermore, we estimated the adsorption behavior of H, NO and NH_3 on NiB monolayer under various applied potentials ranges from -0.5 V to 0.5 V. The corresponding adsorption free energies for H, NO, and NH_3 on their most stable adsorption sites are plotted in Fig. 4. Clearly, the adsorption of H atom on NiB monolayer is still very weak and NO adsorption is stronger than that of NH_3 in the range of -0.5 V to 0.1 V. By controlling the applied potential, it is feasible to ensure that the adsorption energy of NO is larger than that of H and NH_3 , achieving the desired selective adsorption.

Simultaneously, strain is a common approach to modulate material properties. In our previous research on NiB monolayer, we observed a topological phase transition as the applied strain varied. Hence, we explore the influence of strain on the adsorption of NO and NH_3 on NiB monolayer. As shown in Fig. S17, the adsorption energy of NO and NH_3 on NiB monolayer increases gradually with the increased strain, and the adsorption energy difference between these two molecules was always greater than 0.6 eV, which ensures the adsorption selectivity of NO.

4. Conclusion

Using density functional theory (DFT) calculations, we systematically investigated the catalytic mechanism of the electrochemical reduction of NO to NH_3 on 2D NiB monolayer. The optimal reaction pathway of NORR for NH_3 production is $^*NO \rightarrow ^*NOH \rightarrow ^*N \rightarrow ^*NH \rightarrow ^*NH_2 \rightarrow ^*NH_3$. It is noteworthy that all steps of the optimal pathway are exothermic and only the hydrogenation of *NH_2 to *NH_3 possesses a low kinetic barrier of 0.16 eV. The selective adsorption of NO is observed at the applied potential of 0 V and the considered strain. Additionally, the rather weak adsorption of H atom and the existence of relative higher energy barriers for N_2O/N_2 generation guarantee the selectivity of NH_3 production. Our results demonstrate that the 2D NiB monolayer is a highly potential NO electroreduction catalyst with high catalytic activity and selectivity towards the synthesis of NH_3 .

CRedit authorship contribution statement

Wengeng Chen: Investigation, Data curation, Writing – original draft, Visualization. **Yaowei Xiang:** Formal analysis. **Zepeng Wu:** Formal analysis. **Meijie Wang:** Formal analysis. **Yimei Fang:** Formal analysis. **Zi-Zhong Zhu:** Writing – review & editing. **Shunqing Wu:** Writing – review & editing. **Xinrui Cao:** Conceptualization, Writing – review & editing.

Declaration of Competing Interest

The authors declare that they have no known competing financial interests or personal relationships that could have appeared to influence the work reported in this paper.

Data availability

Data will be made available on request.

Acknowledgments

This work is supported by the National Natural Science Foundation of China (22073076 and 21933009) and the Fundamental Research Funds for the Central Universities of China (20720210023). The Xiamen University's High-Performance Computing Center is acknowledged for the computational resources. Shaorong Fang and Tianfu Wu from Information and Network Center of Xiamen University are acknowledged for the help with the GPU computing.

Appendix A. Supplementary data

Supplementary data to this article can be found online at <https://doi.org/10.1016/j.apsusc.2023.157887>.

References

- [1] T. Mou, J. Liang, Z.Y. Ma, L.C. Zhang, Y.T. Lin, T.S. Li, Q. Liu, Y.L. Luo, Y. Liu, S. Y. Gao, H.T. Zhao, A.M. Asiri, D.W. Ma, X.P. Sun, High-efficiency electrohydrogenation of nitric oxide to ammonia on a Ni_2P nanoarray under ambient conditions, *J. Mater. Chem. A* 9 (2021) 24268–24275.
- [2] V.I. Parvulescu, P. Grange, B. Delmon, Catalytic removal of NO, *Catal. Today* 46 (1998) 233–316.
- [3] D.M. Meng, W.C. Zhan, Y. Guo, Y.L. Guo, L. Wang, G.Z. Lu, A Highly Effective Catalyst of Sm-MnO_x for the NH_3 -SCR of NO_x at Low Temperature: Promotional Role of Sm and Its Catalytic Performance, *ACS Catal.* 5 (2015) 5973–5983.
- [4] N.Y. Topsoe, Mechanism of the Selective Catalytic Reduction of Nitric-Oxide by Ammonia Elucidated by in-Situ Online Fourier-Transform Infrared-Spectroscopy, *Science* 265 (1994) 1217–1219.
- [5] M. Koebel, G. Madia, M. Elsener, Selective catalytic reduction of NO and NO₂ at low temperatures, *Catal. Today* 73 (2002) 239–247.
- [6] J. Li, H. Chang, L. Ma, J. Hao, R.T. Yang, Low-temperature selective catalytic reduction of NO_x with NH₃ over metal oxide and zeolite catalysts-A review, *Catal. Today* 175 (2011) 147–156.
- [7] S.H. Zhou, B. Varughese, B. Eichhorn, G. Jackson, K. McIlwrath, Pt-Cu core-shell and alloy nanoparticles for heterogeneous NO_x reduction: Anomalous stability and reactivity of a core-shell nanostructure, *Angew. Chem. Int. Ed.* 44 (2005) 4539–4543.
- [8] J.N. Galloway, A.R. Townsend, J.W. Erisman, M. Bekunda, Z.C. Cai, J.R. Freney, L. A. Martinelli, S.P. Seitzinger, M.A. Sutton, Transformation of the nitrogen cycle: Recent trends, questions, and potential solutions, *Science* 320 (2008) 889–892.
- [9] B.H.R. Suryanto, H.L. Du, D.B. Wang, J. Chen, A.N. Simonov, D.R. MacFarlane, Challenges and prospects in the catalysis of electroreduction of nitrogen to ammonia, *Nat. Catal.* 2 (2019) 290–296.
- [10] T. Kandemir, M.E. Schuster, A. Senyshyn, M. Behrens, R. Schlogl, The Haber-Bosch Process Revisited: On the Real Structure and Stability of “Ammonia Iron” under Working Conditions, *Angew. Chem. Int. Ed.* 52 (2013) 12723–12726.
- [11] J.G. Chen, R.M. Crooks, L.C. Seefeldt, K.L. Bren, R.M. Bullock, M.Y. Darensbourg, P.L. Holland, B. Hoffman, M.J. Janik, A.K. Jones, M.G. Kanatzidis, P. King, K. M. Lancaster, S.V. Lymar, P. Pfrohm, W.F. Schneider, R.R. Schrock, Beyond fossil fuel-driven nitrogen transformations, *Science* 360 (2018) 6391.
- [12] S.L. Foster, S.I.P. Bakovic, R.D. Duda, S. Maheshwari, R.D. Milton, S.D. Minteer, M. J. Janik, J.N. Renner, L.F. Greenlee, Catalysts for nitrogen reduction to ammonia, *Nat. Catal.* 1 (2018) 490–500.
- [13] C.X. Guo, J.R. Ran, A. Vasileff, S.Z. Qiao, Rational design of electrocatalysts and photo(electro) catalysts for nitrogen reduction to ammonia (NH₃) under ambient conditions, *Energ Environ. Sci.* 11 (2018) 45–56.
- [14] G. Soloveichik, Electrochemical synthesis of ammonia as a potential alternative to the Haber-Bosch process, *Nat. Catal.* 2 (2019) 377–380.
- [15] V. Kordali, G. Kyriacou, C. Lambrou, Electrochemical synthesis of ammonia at atmospheric pressure and low temperature in a solid polymer electrolyte cell, *ChemCommun* (2000) 1673–1674.
- [16] X. Liu, Z.X. Wang, J. Zhao, J.X. Zhao, Y.J. Liu, Two-dimensional π -conjugated osmium bis(dithiolene) complex (OsC₄S₄) as a promising electrocatalyst for ambient nitrogen reduction to ammonia, *Appl. Surf. Sci.* 487 (2019) 833–839.
- [17] L.M. Azofra, N. Li, D.R. MacFarlane, C.H. Sun, Promising prospects for 2D d²-d⁴ M₃C₂ transition metal carbides (MXenes) in N₂ capture and conversion into ammonia, *Energ Environ. Sci.* 9 (2016) 2545–2549.
- [18] S. Han, X. Wei, Y. Huang, J. Zhang, J. Yang, Z. Wang, Tuning the activity and selectivity of nitrogen reduction reaction on double-atom catalysts by B doping: A density functional theory study, *Nano Energy* 99 (2022), 107363.
- [19] Y.W. Xiang, L. Li, Y.M. Li, Z.Z. Zhu, S.Q. Wu, X.R. Cao, High-density Fe single atoms anchored on 2D-Fe₂C₁₂ monolayer materials for N₂ reduction to NH₃ with high activity and selectivity, *Appl. Surf. Sci.* 602 (2022) 154380.
- [20] A.R. Singh, B.A. Rohr, M.J. Statt, J.A. Schwalbe, M. Cargnello, J.K. Nørskov, Strategies toward Selective Electrochemical Ammonia Synthesis, *ACS Catal.* 9 (2019) 8316–8324.
- [21] G.F. Chen, S. Ren, L. Zhang, H. Cheng, Y. Luo, K. Zhu, L.X. Ding, H. Wang, Advances in Electrocatalytic N₂ Reduction-Strategies to Tackle the Selectivity Challenge, *Small Methods* 3 (2018) 1800337.

- [22] A.R. Singh, B.A. Rohr, J.A. Schwalbe, M. Cargnello, K. Chan, T.F. Jaramillo, I. Chorkendorff, J.K. Nørskov, Electrochemical Ammonia Synthesis-The Selectivity Challenge, *ACS Catal.* 7 (2017) 706–709.
- [23] J. Long, S.M. Chen, Y.L. Zhang, C.X. Guo, X.Y. Fu, D.H. Deng, J.P. Xiao, Direct Electrochemical Ammonia Synthesis from Nitric Oxide, *Angew. Chem. Int. Ed.* 59 (2020) 9711–9718.
- [24] Q. Wu, H. Wang, S.Y. Shen, B.B. Huang, Y. Dai, Y.D. Ma, Efficient nitric oxide reduction to ammonia on a metal-free electrocatalyst, *J. Mater. Chem. A* 9 (2021) 5434–5441.
- [25] D.H. Kim, S. Ringe, H. Kim, S. Kim, B. Kim, G. Bae, H.S. Oh, F. Jaouen, W. Kim, H. Kim, C.H. Choi, Selective electrochemical reduction of nitric oxide to hydroxylamine by atomically dispersed iron catalyst, *Nat. Commun.* 12 (2021) 1856.
- [26] I. Katsounaros, M.C. Figueiredo, X.T. Chen, F. Calle-Vallejo, M.T.M. Koper, Structure- and Coverage-Sensitive Mechanism of NO Reduction on Platinum Electrodes, *ACS Catal.* 7 (2017) 4660–4667.
- [27] C.A. Farberow, J.A. Dumesic, M. Mavrikakis, Density Functional Theory Calculations and Analysis of Reaction Pathways for Reduction of Nitric Oxide by Hydrogen on Pt(111), *ACS Catal.* 4 (2014) 3307–3319.
- [28] J. Choi, H.L. Du, C.K. Nguyen, B.H.R. Suryanto, A.N. Simonov, D.R. MacFarlane, Electroreduction of Nitrates, Nitrites, and Gaseous Nitrogen Oxides: A Potential Source of Ammonia in Dinitrogen Reduction Studies, *ACS Energy Lett.* 5 (2020) 2095–2097.
- [29] P. Shi, D.L. Pang, Z.Y. Zhang, L. Lin, C.Z. He, Transition metals embedded Pt (100) surface as an electrocatalysts for NO reduction reaction: A first-principles study, *Appl. Surf. Sci.* 619 (2023), 156744.
- [30] H. Niu, Z.F. Zhang, X.T. Wang, X.H. Wan, C.G. Kuai, Y.Z. Guo, A Feasible Strategy for Identifying Single-Atom Catalysts Toward Electrochemical NO-to-NH₃ Conversion, *Small* 17 (2021) 2102396.
- [31] S.Q. Liu, Y.W. Liu, Z.W. Cheng, X.P. Gao, Y.J. Tan, Z.M. Shen, T. Yuan, Two-dimensional transition metal phthalocyanine sheet as a promising electrocatalyst for nitric oxide reduction: a first principle study, *Environ. Sci. Pollut. Res.* 28 (2021) 7191–7199.
- [32] N. Saeidi, M.D. Esrafilii, J.J. Sardroodi, NO electrochemical reduction over Si-N₄ embedded graphene: A DFT investigation, *Appl. Surf. Sci.* 544 (2021), 148869.
- [33] Q. Wu, W. Wei, X.S. Lv, Y.Y. Wang, B.B. Huang, Y. Dai, Cu@g-C₃N₄: An Efficient Single-Atom Electrocatalyst for NO Electrochemical Reduction with Suppressed Hydrogen Evolution, *J. Phys. Chem. C* 123 (2019) 31043–31049.
- [34] S. Ji, J.X. Zhao, Boron-doped graphene as a promising electrocatalyst for NO electrochemical reduction: a computational study, *New J. Chem.* 42 (2018) 16346–16353.
- [35] Y.M. Zang, Q. Wu, S.H. Wang, B.B. Huang, Y. Dai, Y.D. Ma, High-Throughput Screening of Efficient Biatom Catalysts Based on Monolayer Carbon Nitride for the Nitric Oxide Reduction Reaction, *J. Phys. Chem. Lett.* 13 (2022) 527–535.
- [36] B.K. Zhang, J. Zhou, Z.M. Sun, MBenes: progress, challenges and future, *J. Mater. Chem. A* 10 (2022) 15865–15880.
- [37] B. Li, Y. Wu, N. Li, X. Chen, X. Zeng, Arramel; Zhao, X.; Jiang, J. Single-Metal Atoms Supported on MBenes for Robust Electrochemical Hydrogen Evolution, *ACS Appl. Mater. Interfaces* 12 (2020) 9261–9267.
- [38] B. Zhang, J. Zhou, Z. Guo, Q. Peng, Z. Sun, Two-dimensional chromium boride MBenes with high HER catalytic activity, *Appl. Surf. Sci.* 500 (2020), 144248.
- [39] T. Zhang, B.K. Zhang, Q. Peng, J. Zhou, Z.M. Sun, Mo₂B₂ MBene-supported single-atom catalysts as bifunctional HER/OER and OER/ORR electrocatalysts, *J. Mater. Chem. A* 9 (2021) 433–441.
- [40] X.L. Liu, Z.X. Liu, H.Q. Deng, Theoretical Evaluation of MBenes as Catalysts for the CO₂ Reduction Reaction, *J. Phys. Chem. C* 125 (2021) 19183–19189.
- [41] Y. Cheng, J. Mo, Y. Li, Y. Zhang, Y. Song, A systematic computational investigation of the water splitting and N₂ reduction reaction performances of monolayer MBenes, *Phys. Chem. Chem. Phys.* 23 (2021) 6613–6622.
- [42] Y. Xiao, C. Shen, Transition-Metal Borides (MBenes) as New High-Efficiency Catalysts for Nitric Oxide Electroreduction to Ammonia by a High-Throughput Approach, *Small* 17 (2021) 2100776.
- [43] Z. Jiang, P. Wang, X. Jiang, J.J. Zhao, MBene (MnB): a new type of 2D metallic ferromagnet with high Curie temperature, *Nanoscale Horiz.* 3 (2018) 335–341.
- [44] Z.G. Li, B.Q. Wei, Topological materials and topologically engineered materials: properties, synthesis, and applications for energy conversion and storage, *J. Mater. Chem. A* 9 (2021) 1297–1313.
- [45] Y. Qie, J.Y. Liu, S. Wang, Q. Sun, P. Jena, Tetragonal C₂₄: a topological nodal-surface semimetal with potential as an anode material for sodium ion batteries, *J. Mater. Chem. A* 7 (2019) 5733–5739.
- [46] R.M. Sattigeri, P.K. Jha, P. Spiewak, K.J. Kurzydowski, Two dimensional LiMgAs: A topological quantum catalyst for hydrogen evolution reaction, *Appl. Phys. Lett.* 121 (2022), 123101.
- [47] X. Zhu, Y. Wang, Y. Jing, T. Heine, Y. Li, beta-PdBi₂ monolayer: two-dimensional topological metal with superior catalytic activity for carbon dioxide electroreduction to formic acid, *Mater. Today Adv.* 8 (2020), 100091.
- [48] Z.B. Ren, H.N. Zhang, S.H. Wang, B.B. Huang, Y. Dai, W. Wei, Nitric oxide reduction reaction for efficient ammonia synthesis on topological nodal-line semimetal Cu₂Si monolayer, *J. Mater. Chem. A* 10 (2022) 8568–8577.
- [49] L.S. Zhao, G.T. Yu, X.R. Huang, W. Chen, TaIrTe₄ Monolayer with Topological Insulator Characteristic: A New and Highly Efficient Electrocatalyst toward Oxygen Reduction Reaction, *J. Phys. Chem. C* 126 (2022) 19685–19692.
- [50] Q.L. Yu, Y.M. Fang, X.R. Cao, S.Q. Wu, Z.Z. Zhu, Strain modulated quantum spin Hall effect in monolayer NiB, *Appl. Phys. Lett.* 118 (2021), 183101.
- [51] G. Bhaskar, V. Gvozdzetskiy, M. Batuk, K.M. Wiaderek, Y. Sun, R.H. Wang, C. Zhang, S.L. Carnahan, X. Wu, R.A. Ribeiro, S.L. Bud'ko, P.C. Canfield, W. Y. Huang, A.J. Rossini, C.Z. Wang, K.M. Ho, J. Hadernmann, J.V. Zaikina, Topochemical Deintercalation of Li from Layered LiNiB: toward 2D MBene, *J. Am. Chem. Soc.* 143 (2021) 4213–4223.
- [52] G. Kresse, J. Furthmuller, Efficiency of ab-initio total energy calculations for metals and semiconductors using a plane-wave basis set, *Comp. Mater. Sci.* 6 (1996) 15–50.
- [53] G. Kresse, J. Furthmuller, Efficient iterative schemes for ab initio total-energy calculations using a plane-wave basis set, *Phys. Rev. B* 54 (1996) 11169–11186.
- [54] P.E. Blöchl, Projector augmented-wave method, *Phys. Rev. B* 50 (1994) 17953.
- [55] J.P. Perdew, K. Burke, M. Ernzerhof, Generalized gradient approximation made simple, *Phys. Rev. Lett.* 77 (1996) 3865–3868.
- [56] S. Grimme, J. Antony, S. Ehrlich, H. Krieg, A consistent and accurate ab initio parametrization of density functional dispersion correction (DFT-D) for the 94 elements H-Pu, *J. Chem. Phys.* 132 (2010), 154104.
- [57] S. Grimme, S. Ehrlich, L. Goerigk, Effect of the Damping Function in Dispersion Corrected Density Functional Theory, *J. Comput. Chem.* 32 (2011) 1456–1465.
- [58] M. Krack, M. Parrinello, All-electron ab-initio molecular dynamics, *Phys. Chem. Chem. Phys.* 2 (2000) 2105–2112.
- [59] G. Henkelman, B.P. Uberuaga, H. Jonsson, A climbing image nudged elastic band method for finding saddle points and minimum energy paths, *J. Chem. Phys.* 113 (2000) 9901–9904.
- [60] J.K. Nørskov, J. Rossmeisl, A. Logadottir, L. Lindqvist, J.R. Kitchin, T. Bligaard, H. Jonsson, Origin of the overpotential for oxygen reduction at a fuel-cell cathode, *J. Phys. Chem. B* 108 (2004) 17886–17892.
- [61] NIST-JANAF Tables. https://janaf.nist.gov/periodic_table.html.
- [62] K. Mathew, R. Sundararaman, K. Letchworth-Weaver, T.A. Arias, R.G. Hennig, Implicit solvation model for density-functional study of nanocrystal surfaces and reaction pathways, *J. Chem. Phys.* 140 (2014), 084106.
- [63] R. Sundararaman, K. Letchworth-Weaver, K.A. Schwarz, D. Gunceler, Y. Ozhobes, T.A. Arias, JDFTx: Software for joint density-functional theory, *Software* 6 (2017) 278–284.
- [64] D. Kim, J.J. Shi, Y.Y. Liu, Substantial Impact of Charge on Electrochemical Reactions of Two Dimensional Materials, *J. Am. Chem. Soc.* 140 (2018) 9127–9131.
- [65] R. Sundararaman, W.A. Goddard III, The charge-asymmetric nonlocally determined local-electric (CANDLE) solvation model, *J. Chem. Phys.* 142 (2015), 064107.
- [66] S.Y. Wu, Y.C. Lin, J.J. Ho, Reaction of NO on Ni-Pt Bimetallic Surfaces Investigated with Theoretical Calculations, *J. Phys. Chem. C* 115 (2011) 7538–7544.
- [67] C.S. Huang, A. Murat, V. Babar, E. Montes, U. Schwingenschlogl, Adsorption of the Gas Molecules NH₃, NO, NO₂, and CO on Borophene, *J. Phys. Chem. C* 122 (2018) 14665–14670.
- [68] X.H. Zhao, Y.Y. Liu, Origin of Selective Production of Hydrogen Peroxide by Electrochemical Oxygen Reduction, *J. Am. Chem. Soc.* 143 (2021) 9423–9428.
- [69] X.H. Zhao, Y.Y. Liu, Unveiling the Active Structure of Single Nickel Atom Catalysis: Critical Roles of Charge Capacity and Hydrogen Bonding, *J. Am. Chem. Soc.* 142 (2020) 5773–5777.
- [70] K. Xie, F.T. Wang, F.F. Wei, J. Zhao, S. Lin, Revealing the Origin of Nitrogen Electroreduction Activity of Molybdenum Disulfide Supported Iron Atoms, *J. Phys. Chem. C* 126 (2022) 5180–5188.
- [71] G.P. Gao, L.W. Wang, Substantial potential effects on single-atom catalysts for the oxygen evolution reaction simulated via a fixed-potential method, *J. Catal.* 391 (2020) 530–538.
- [72] M. Tursun, C. Wu, Vacancy-triggered and dopant-assisted NO electrocatalytic reduction over MoS₂, *Phys. Chem. Chem. Phys.* 23 (2021) 19872–19883.
- [73] M. Tursun, C. Wu, NO Electroreduction by Transition Metal Dichalcogenides with Chalcogen Vacancies, *ChemElectroChem* 8 (2021) 3113–3122.
- [74] C.A. Casey-Stevens, H. Asmundsson, E. Skulason, A.L. Garden, A density functional theory study of the mechanism and onset potentials for the major products of NO electroreduction on transition metal catalysts, *Appl. Surf. Sci.* 552 (2021), 149063.
- [75] A. Clayborne, H.J. Chun, R.B. Rankin, J. Greeley, Elucidation of Pathways for NO Electroreduction on Pt(111) from First Principles, *Angew. Chem. Int. Ed.* 54 (2015) 8255–8258.
- [76] H.J. Chun, V. Apaja, A. Clayborne, K. Honkala, J. Greeley, Atomistic Insights into Nitrogen-Cycle Electrochemistry: A Combined DFT and Kinetic Monte Carlo Analysis of NO Electrochemical Reduction on Pt(100), *ACS Catal.* 7 (2017) 3869–3882.
- [77] Q. Zhou, F. Gong, Y.L. Xie, D.W. Xia, Z.G. Hu, S.J. Wang, L.S. Liu, R. Xiao, A general strategy for designing metal-free catalysts for highly-efficient nitric oxide reduction to ammonia, *Fuel* 310 (2022), 122442.
- [78] N. Saeidi, M.D. Esrafilii, J. Jahanbin Sardroodi, Electrochemical reduction of NO catalyzed by boron-doped C₆₀ fullerene: a first-principles study, *Rsc Adv.* 12 (2022) 3003–3012.
- [79] S. Liu, G. Xing, J.-Y. Liu, Computational screening of single-atom catalysts for direct electrochemical NH₃ synthesis from NO on defective boron phosphide monolayer, *Appl. Surf. Sci.* 611 (2023), 155764.
- [80] X.Y. Guo, J.X. Gu, S.R. Lin, S.L. Zhang, Z.F. Chen, S.P. Huang, Tackling the Activity and Selectivity Challenges of Electrocatalysts toward the Nitrogen Reduction Reaction via Atomically Dispersed Biatom Catalysts, *J. Am. Chem. Soc.* 142 (2020) 5709–5721.
- [81] K.A. Nguyen, M.S. Gordon, J.A. Montgomery, H.H. Michels, Structures, Bonding, and Energetics of N₂O₂ Isomers, *J. Phys. Chem.* 98 (1994) 10072–10078.